Thermophysical Properties of BiFeO3, Bi0.91Nd0.09FeO3, and BiFe0.91Mn0.09O3 Multiferroics at High Temperatures

Article *in* Physics of the Solid State · June 2016

DOI: 10.1134/S1063783416060226

2 authors:

Andrei Klyndyuk
Belarusian State Technological University
103 PUBLICATIONS **375** CITATIONS

SEE PROFILE

Alexander Khort
KTH Royal Institute of Technology
38 PUBLICATIONS **93** CITATIONS

SEE PROFILE

ISSN 1063-7834, Physics of the Solid State, 2016, Vol. 58, No. 6, pp. 1285–1288. © Pleiades Publishing, Ltd., 2016.
Original Russian Text © A.I. Klyndyuk, A.A. Khort, 2016, published in Fizika Tverdogo Tela, 2016, Vol. 58, No. 6, pp. 1243–1246.

THERMAL PROPERTIES

Thermophysical Properties of $BiFeO_3$, $Bi_{0.91}Nd_{0.09}FeO_3$, and $BiFe_{0.91}Mn_{0.09}O_3$ Multiferroics at High Temperatures

A. I. Klyndyuk* and A. A. Khort

Belarusian State Technological University, Sverdlova str. 13a, Minsk, 220006 Belarus

**e-mail: klyndyuk@belstu.by*

Received November 3, 2015; in final form, November 12, 2015

Abstract—The thermal diffusion, heat capacity, and thermal conductivity of $BiFeO_3$, $Bi_{0.91}Nd_{0.09}FeO_3$, and $BiFe_{0.91}Mn_{0.09}O_3$ multiferroics have been studied at high temperatures (300–1120 K). The dominant mechanisms of phonon transfer in the regions of the antiferromagnetic and ferroelectric phase transitions have been determined. The temperature dependence of the mean free path of phonons has been found.

DOI: 10.1134/S1063783416060226

1. INTRODUCTION

In recent years, bismuth orthoferrite $BiFeO_3$ having extremely high temperatures of the antiferromagnetic ($T_N \approx 643$ K) and ferroelectric ($T_C \approx 1083$ K) ordering are considered as a promising basis for developing new-generation multiferroics intended for designing magnetic field sensors, devices of information recording/reading, spintronics, microwave, and other apparatuses [1]. At room temperature, $BiFeO_3$ has a rhombohedrally distorted perovskite structure (space group of symmetry $R3c$), close to a cubic structure. At temperatures lower than T_N, bismuth orthoferrite has a complex spatially modulated magnetic structure of the cycloid type that is incommensurate with its crystalline structure and, as a result, it does not exhibit a linear magnetoelectric effect and demonstrates only a significantly weaker quadratic magnetoelectric effect [2, 3]. The spatially modulated spin structure in $BiFeO_3$ can be destructed in strong magnetic fields [3], by nanostructuring [2, 3], and also by partial substitution of transition metal ions for iron ions [2, 4, 5] or rare-earth metal ions for bismuth ions [2, 3, 6, 7]; in this case, the latter substitution also increases the spontaneous polarization and the magnetization of the formed solid solutions (SS) [2, 7].

The crystal structure, the magnetic and electrical properties of $BeFeO_3$ and solid solutions on its base were studied in many work (e.g., reviews [2, 3, 8]); however, the thermophysial properties of these materials are scantily known. The heat capacity of bismuth orthoferrite $BiFeO_3$ and its solid solutions with rare-earth metals $Bi_{0.95}Re_{0.05}FeO_3$ (Re = La, Eu, Ho), and $Bi_{1-x}Gd_xFeO_3$ ($0.05 < x < 0.20$) were studied in [9–11]. The thermal expansion of ferrites $BiFeO_3$ and $Bi_{0.95}La_{0.05}FeO_3$ were studied in [9, 12] and the thermal diffusion and the thermal conductivity of these multiferroics at elevated temperatures were described in [13].

In this work, we present the results of studying the thermal diffusion, the heat capacity, and the thermal conductivity of bismuth orthoferrite $BiFeO_3$ and its solid solutions $Bi_{0.91}Nd_{0.09}FeO_3$ and $BiFe_{0.91}Mn_{0.09}O_3$ in a wide temperature range (300–1120 K) including regions of high-temperature phase transitions (antiferromagnetic and ferroelectric).

2. SAMPLE PREPARATION AND EXPERIMENTAL TECHNIQUE

Multiferroics $BiFeO_3$, $Bi_{0.91}Nd_{0.09}FeO_3$, and $BiFe_{0.91}Mn_{0.09}O_3$ ceramic samples were synthesized by solid-phase reaction method from chemical pure Bi_2O_3, Nd_2O_3 (NO–L), Fe_2O_3 (analytical pure 2-4), and Mn_2O_3 (analytical pure 11-2) in air at a temperature of 1073 K (8 h) with subsequent sintering in air at temperatures 1083–1113 K (5–10 h) [14]. The X-ray powder diffraction studies of grinded ceramic sinters were performed using a Bruker D8 XRD diffractometer, CuK_α radiation, and a Ni filter. The results showed that the ferrite prepared crystallized, at room temperature, in the rhombohedral syngony (space group of symmetry $R3c$) with the unit cell parameters a = 0.5576(2), 0.5579(3), and 0.5579(3) nm and c = 1.386(1), 1.383(1), and 1.384(1) nm (hexagonal setting) for $BiFeO_3$, $Bi_{0.91}Nd_{0.09}FeO_3$, and $BiFe_{0.91}Mn_{0.09}O_3$, respectively, which agrees well with available data [2, 5, 7]. The effective density ρ of the sintered ceramics was found from the mass and the geometric sizes of the samples.

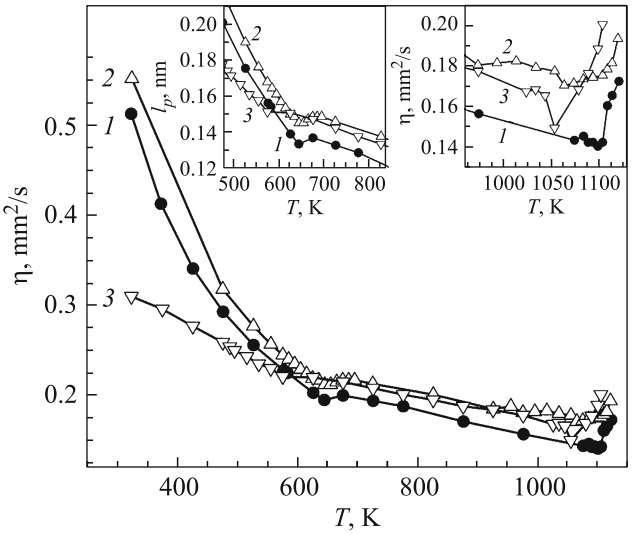

Fig. 1. Temperature dependences of the thermal diffusion of ceramics' (*1*) $BiFeO_3$, (*2*) $Bi_{0.91}Nd_{0.09}FeO_3$, and (*3*) $BiFe_{0.91}Mn_{0.09}O_3$. The inserts show the temperature dependences of (the left insert) the mean phonon free path near the antiferromagnetic transition and (the right insert) the thermal diffusion near the ferroelectric transition.

The thermal diffusion (TD) η of the ceramics was studied by the laser flash using a NETZSCH (Germany) LFA-457 MicroFlash in the temperature range of 320–1120 K in an Ar atmosphere in pulsed mode. The 3-mm-thick samples were 12.6 mm in diameter. Before the measurements, the samples were polished, and heat-conducting graphite conducting coating was deposited on the sample ends. The results of measurements were treated by the Netzsch Proteus LFA Analysis software using the Cape–Lemon mathematical model taking into account the correction of the basis line. The unit was preliminarily calibrated using the reference "pyroceram" (NETZSCH) samples (the detector type was InSb).

Heat capacity C_p of the powder samples was measured using a NETZSCH (Germany) DSC 404 F3 Pegasus differential scanning calorimeter in the temperature range of 300–1000 K at a heating rate of 20 K min^{-1} in an Ar atmosphere. The powders were preliminarily calcined at the maximum temperature of the experiment, cooled, and, thereafter, the DSC curves were recorded. The heat capacity of the ferrites was calculated using the values of the standard heat capacity of sapphire (NETZSCH). The DSC curves were treated using the Netzsch Proteus Thermal Analysis program package. The heats of the phase transitions proceeding in the materials under study were calculated from the integral areas of peaks in the DSC curves taking into account the basis line using the Laplas model and the NETZSCH PeakSeparation 3 program package.

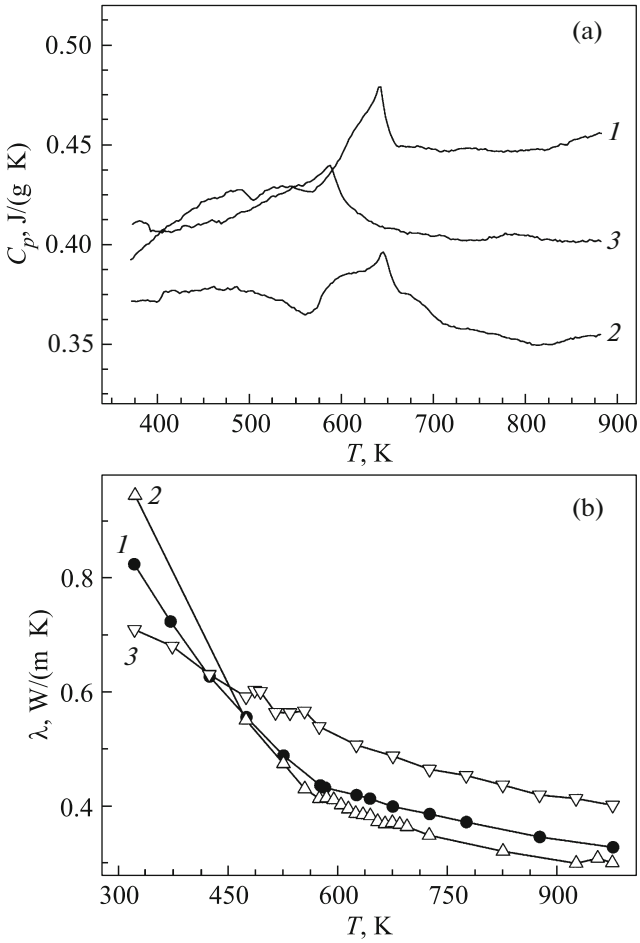

Fig. 2. Temperature dependences of (a) the specific heat and (b) the thermal conductivity of ferrites (*1*) $BiFeO_3$, (*2*) $Bi_{0.91}Nd_{0.09}FeO_3$, and (*3*) $BiFe_{0.91}Mn_{0.09}O_3$.

The thermal conductivity λ of the samples was calculated by formula $\lambda = \eta\rho C_p$ using the experimental values of their thermal diffusion, effective density, and heat capacity.

3. RESULTS AND DISCUSSION

Figures 1 and 2 depict the temperature dependences of the thermal diffusion, the heat capacity, and the thermal conductivity of ferrites $BiFeO_3$, $Bi_{0.91}Nd_{0.09}FeO_3$, and $BiFe_{0.91}Mn_{0.09}O_3$ in the temperature range of 300–1120 K. The dependences have noticeable anomalies near the temperatures of the antiferromagnetic (T_N = 588–649 K) and ferroelectric (T_C = 1053–1098 K) phase transitions (table).

To analyze temperature dependences $\eta(T)$ and $\lambda(T)$, we calculated the mean phonon free paths l_p in the materials under study using expressions

$$\eta = (1/3)v_s l_p \lambda_p = (1/3)C_v v_s l_p.$$

Here, v_s is the sound velocity, l_p is the phonon component of the thermal conductivity, and C_v is the isochoric heat capacity of the unit volume. We determined η, λ_p, and C_v experimentally ($\lambda_p \approx \lambda$), since, according to the data from [14] for bismuth orthoferrite and its derivatives, the electron component of the thermal conductivity is much lower than the phonon component ($\lambda_e \ll \lambda_p$); $C_v \approx C_p\rho$, where C_p is the isobaric heat capacity of unit mass calculated from the DSC data for the samples); the data on the sound velocity were taken from [15].

Independent estimations of l_p from the measurements of the thermal diffusion and the thermal conductivity gave the same values ($l_p \approx 0.12$–0.15 nm at $T > T_N$) and the same temperature dependence of l_p (the left insert in Fig. 1). Taking into account the found values of l_p, we can neglect the phonon scattering by the boundaries of crystallites several micrometers in size [16], since $l_p \ll d$, where d is the mean crystallite size. Thus, the scattering centers (structural distortions), limiting the phonon heat transfer in bismuth orthoferrite-based multiferroics, have sizes on the order of the lattice parameter, and such centers can be various local distortions of the crystal structure, in particular, Jahn–Teller distortions of the oxygen octahedrons (FeO_6) that are substantially changed during phase transitions and also under various external actions [17].

As is seen from Fig. 1, the thermal diffusion of ferrites $BiFeO_3$, $Bi_{0.91}Nd_{0.09}FeO_3$, and $BiFe_{0.91}Mn_{0.09}O_3$ slightly decreased in the temperature range $T_N < T < T_C$, which seems to be related to the increase in the number of the phonon scattering centers with temperature because of the lattice distortions, which, according to the neutron diffraction data [18], are due to the rotation of oxygen octahedrons (FeO_6) and "polar" displacement of ions Bi^{3+} (Nd^{3+}) and Fe^{3+} (Mn^{3+}) from their positions in the perfect perovskite structure.

The thermal diffusion had a minimum near the ferroelectric phase transition (the right insert in Fig. 1), which is due to the changes in both the sound velocity and the phonon free path, since $\eta = (1/3)v_s l_p$. It is known that the transitions are accompanied by a minimum of the sound propagation velocity and a sound absorption peak because of the interaction between the strain (caused by the sound wave) and the spontaneous polarization (relaxation absorption) and the interaction of the sound wave with thermal fluctuations of the polarization (fluctuation absorption) [19]. The ferroelectric phase transition temperatures of solid solutions $Bi_{0.91}Nd_{0.09}FeO_3$ and $BiFe_{0.91}Mn_{0.09}O_3$ decreased by 35 and 45 K, respectively (table and the right insert in Fig. 1). The transition of multiferroics $BiFeO_3$, $Bi_{0.91}Nd_{0.09}FeO_3$, and $BiFe_{0.91}Mn_{0.09}O_3$ from the polar rhombohedral (space group *R*3*c*) to the nonpolar orthorhombic (space group *Pbnm*) phase (the ferroelectric → paraelectric phase transition) removed the crystal lattice distortions [18] and led to the lattice compression [2, 12]; as a result, the number of phonon scattering centers decreased and the phonon free paths and the thermal diffusion in the samples increased at $T > T_C$ (the right insert in Fig. 1).

Phase transition temperatures and heats of ferrites $BiFeO_3$, $Bi_{0.91}Nd_{0.09}FeO_3$, and $BiFe_{0.91}Mn_{0.09}O_3$

Ferrite	AFM ↔ PM			FE ↔ PE
	T_N, K		ΔH, J/mol	T_C, K (TD)
	TD	DSC		
$BiFeO_3$	643	643	396	1098
$Bi_{0.91}Nd_{0.09}FeO_3$	649	646	327	1063
$BiFe_{0.91}Mn_{0.09}O_3$	595	588	266	1053

AFM is antiferromagnet, PM is paramagnet, FE is ferroelectric, and PE is paraelectric.

At $T < T_N$, the thermal diffusion and the thermal conductivity of the ferrites increased as temperature decreased (Figs. 1, 2b). This phenomenon is characteristic of dielectric materials and is caused by a sharp increase in the phonon free path (the left insert in Fig. 1), since the transition to a magnetically ordered phase is accompanied by removing the Jahn–Teller distortions [20] and lattice compression [9]. In the vicinity of T_N, dependences $\eta(T)$ of ferrites $BiFeO_3$, $Bi_{0.91}Nd_{0.09}FeO_3$, and $BiFe_{0.91}Mn_{0.09}O_3$ had a minimum that is less noticeable in solid solution $BiFe_{0.91}Mn_{0.09}O_3$ (Fig. 1).

As is seen from the data shown in Fig. 2a and in the table, a partial substitution of neodymium for bismuth in $BiFeO_3$ increased and a partial substitution of manganese for iron in this ferrite decreased its transition temperature from the antiferromagnetic to the paramagnetic state (the antiferromagnetic–paramagnetic phase transition), which agrees well with the data of [2, 9, 11, 13, 16, 21]. The solid solution also demonstrated the decrease in the heat of this transition, which is more noticeable in the solid solution containing Mn.

4. CONCLUSIONS

Thus, in this work, we studied the thermophysical properties (the thermal diffusion, the heat capacity, and the thermal conductivity) of multiferroics $BiFeO_3$, $Bi_{0.91}Nd_{0.09}FeO_3$, and $BiFe_{0.91}Mn_{0.09}O_3$ at high temperatures (300–1120 K). An analysis of the results in combination with the available literature data of the structural and acoustic studies made it possible to conclude that the dominant phonon scattering centers in the bismuth orthoferrite-based materials were local distortions of the crystal structure caused by rotation of oxygen octahedra (FeO_6) and displace-

ments of ions Bi^{3+} (Nd^{3+}) and Fe^{3+} (Mn^{3+}) from their positions in the perfect perovskite structure. We calculated the heats of the antiferromagnetic → paramagnetic phase transition for ferrites $BiFeO_3$, $Bi_{0.91}Nd_{0.09}FeO_3$, and $BiFe_{0.91}Mn_{0.09}O_3$.

ACKNOWLEDGMENTS

This study was supported by the Belarusian Republican Foundation for Fundamental Research (project nos. Kh13-005 and Kh16R-149).

REFERENCES

1. G. A. Smolenskii and V. M. Yudin, Sov. Phys. Solid State **6**, 2937 (1965).
2. G. Catalan and J. F. Scott, Adv. Mater. (Weinheim) **21**, 2463 (2009).
3. A. P. Pyatakov and A. K. Zvezdin, Phys.—Usp. **55** (6), 557 (2012).
4. A. Kumar and K. L. Yadav, J. Phys. Chem. Solids **72**, 1189 (2011).
5. L. Chen, L. Zheng, Y. He, J. Zhang, Z. Mao, and X. Chen, J. Alloys Compd. **633**, 216 (2015).
6. I. O. Troyanchuk, D. V. Karpinsky, M. V. Bushinsky, O. S. Mantytskaya, N. V. Tereshko, and V. N. Shut, J. Am. Ceram. Soc. **94**, 4502 (2011).
7. A. Srivastava, H. K. Singh, V. P. S. Awana, and O. N. Srivastava, J. Alloys Compd. **552**, 336 (2013).
8. M. S. Bernardo, Bol. Soc. Esp. Ceram. Vidrio **53**, 1 (2014).
9. A. A. Amirov, A. B. Batdalov, S. N. Kallaev, Z. M. Omarov, I. A. Verbenko, O. N. Razumovskaya, L. A. Reznichenko, and L. A. Shilkina, Phys. Solid State **51** (6), 1189 (2009).
10. S. A. Kallaev, R. G. Mitarov, Z. M. Omarov, G. G. Gadzhiev, and L. A. Reznichenko, J. Exp. Theor. Phys. **118** (2), 279 (2014).
11. S. N. Kallaev, Z. M. Omarov, R. G. Mitarov, A. R. Bilanov, G. G. Gadzhiev, L. A. Reznichenko, R. M. Ferzilaev, and S. A. Sadykov, Phys. Solid State **56** (7), 1412 (2014).
12. S. M. Selbach, T. Tybell, M.-A. Einarsrud, and T. Grande, J. Solid State Chem. **183**, 1205 (2010).
13. S. N. Kallaev, A. G. Bakmaev, and L. A. Reznichenko, JETP Lett. **97** (8), 470 (2013).
14. A. I. Klyndyuk and E. A. Chizhova, Glass Phys. Chem. **41** (4), 421 (2015).
15. E. P. Smirnova, A. Sotnikova, S. Ktitorov, N. Zaitseva, H. Schmidt, and M. Weihnacht, Eur. Phys. J. B **83**, 39 (2011).
16. A. I. Klyndyuk, E. A. Chizhova, E. A. Tugova, A. I. Galyas, and S. V. Trukhanov, Izv. St. Peterb. Gos. Tekhnol. Inst. (Tekh. Univ.), No. 29, 3 (2015).
17. P. G. Radaelli, M. Marezio, H. Y. Hwang, S.-W. Cheong, and B. Batlogg, Phys. Rev. B: Condens. Matter **54**, 8992 (1996).
18. D. C. Arnold, K. S. Knight, F. D. Morrison, and P. Lightfoot, Phys. Rev. Lett. **102**, 027602 (2009).
19. R. Blinc and B. Zeks, *Soft Modes in Ferroelectrics and Antiferroelectrics* (North-Holland, Amsterdam, 1974; Mir, Moscow, 1975).
20. H. Fujishiro, S. Sugawara, and M. Ikebe, Physica B (Amsterdam) **316–317**, 331 (2002).
21. S. M. Selbach, T. Tybell, M.-A. Einarsrud, and T. Grande, Chem. Mater. **21**, 5176 (2009).

Translated by Yu. Ryzhkov